Research Square

Preprints are preliminary reports that have not undergone peer review.
They should not be considered conclusive, used to inform clinical practice,
or referenced by the media as validated information.

Competitive adsorption of aminomethylphosphonic acid and phosphate on 6-line ferrihydrite: Experimental and surface complexation modeling study

Shu Chen
Southwest University of Science and Technology
Jing Liu
liujing-vip@163.com
Southwest University

Research Article

Keywords: Ferrihydrite, Adsorption, Phosphate, Aminomethylphosphonic acid, Surface complexation model

Posted Date: November 18th, 2026

DOI: https://doi.org/10.21203/rs.3.rs-11031841/v1

License: This work is licensed under a Creative Commons Attribution 4.0 International License.
Read Full License

Additional Declarations: No competing interests reported.

Competitive adsorption of aminomethylphosphonic acid and phosphate on 6-line ferrihydrite: Experimental and surface complexation modeling study

Shu Chen[a], Jing Liu[b,*]

[a]Tianfu Institute of Research and Innovation, Southwest University of Science and Technology, Chengdu, 610299, China

[b]College of Resources and Environment, Southwest University, Chongqing, 400716, China. Tel: +86(023)-68251249

[a]College of Resources and Environment, Southwest University, Chongqing, 400716, China. Tel: +86(023)-68251249

[b]Tianfu Institute of Research and Innovation, Southwest University of Science and Technology, Chengdu, 610299, China

Date: 14 September 2026

Submitted to: Water, Air, & Soil Pollution

Keywords: Ferrihydrite, Adsorption, Phosphate, Aminomethylphosphonic acid, Surface complexation model

* Corresponding author: Liujing-vip@163.com (LIU JING)

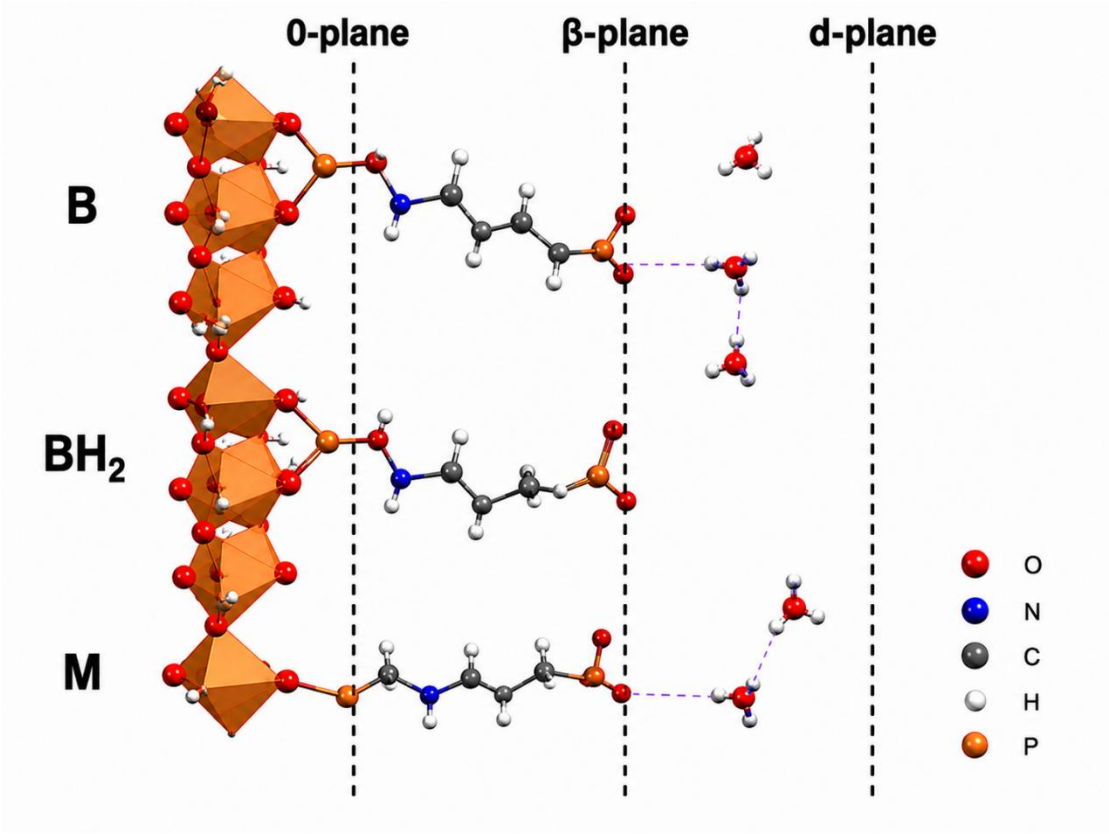
Abstract

Aminomethylphosphonic acid (AMPA) is a persistent degradation product of various organophosphonates. Its environmental transport is regulated not only by adsorption onto metal (hydr)oxides in soils and sediments but also by competitive interactions with phosphate. In this study, competitive batch adsorption experiments of AMPA and phosphate were conducted on synthetic 6-line ferrihydrite over a pH range of 3.5-10.5 and initial concentrations ranging from 0.130 to 1.07 mM to systematically investigate their adsorption behavior at the ferrihydrite-water interface. The adsorption edge data were interpreted using the charge distribution (CD)-MUSIC model to derive the corresponding intrinsic equilibrium constants. By accounting for both surface electrostatic interactions and chemical affinity, the model successfully predicted the competitive adsorption behavior of AMPA and phosphate. The adsorption of AMPA on ferrihydrite was dominated by three surface complexes: a bidentate binuclear complex (B), a protonated bidentate binuclear complex (BH), and a protonated monodentate mononuclear complex (MH), with intrinsic equilibrium constants (log K) of 27.9 ± 0.10, 25.2 ± 0.10, and 17.1 ± 0.1, respectively. Within the investigated concentration range, the presence of phosphate reduced the adsorption of AMPA on ferrihydrite by 4.0%-25%. Compared with phosphate, AMPA exhibited a substantially stronger affinity for the ferrihydrite surface, with the maximum adsorbed amount reaching 1.69 times that of phosphate under identical initial concentrations. The adsorption behavior in the competitive system was governed by the coupled effects of competitive inhibition and surface electrostatic promotion rather than by direct

competition alone. Consequently, the adsorption percentages of both species were not determined solely by their initial concentrations, resulting in enhanced mobility of AMPA in competitive systems. This study provides a quantitative description of AMPA adsorption on ferrihydrite based on the CD-MUSIC model and offers mechanistic insights and thermodynamic parameters for predicting the environmental fate and transport of organophosphonates.

Keywords: Ferrihydrite, Adsorption, Phosphate, Aminomethylphosphonic acid, Surface complexation model

Graphical Abstract



1. Introduction

Organic phosphonates are widely used in agriculture, particularly as herbicides. Aminomethylphosphonic acid (AMPA) is the major degradation product of several organophosphonate herbicides, most notably glyphosate (Barrett and McBride, 2005; Li et al., 2016; Trinh et al., 2026), and is also an important environmental transformation product of other phosphonate compounds (Borggaard and Gimsing, 2008). Owing to its high persistence and widespread occurrence in natural environments, AMPA has frequently been detected in soils, surface waters, and groundwater (Grandcoin et al., 2017; Lescano et al., 2018).

Compared with glyphosate, AMPA lacks the carboxyl group while retaining both the phosphonate and amino functional groups, making it an important intermediate linking organophosphorus compounds and inorganic phosphate in the environment. To date, most studies have focused on the adsorption behavior and environmental fate of glyphosate (Singh and Walker, 2006; Sun et al., 2019; Ruffolo et al., 2023; Villalobos-Lara et al., 2026), whereas the adsorption mechanism of AMPA has received considerably less attention, and its molecular-scale surface complexation mechanism remains largely unknown.

Ferrihydrite is one of the most reactive iron oxides in soils, sediments, and engineered water treatment systems, and plays a crucial role in controlling the mobility of phosphonates and phosphate (RAMPAzzo et al., 2013; Pereira et al., 2019; Zhang et al., 2026). It is therefore considered a key mineral for investigating the environmental

behavior of AMPA. Owing to its large specific surface area and abundant reactive surface hydroxyl groups, ferrihydrite provides numerous adsorption sites for phosphorus-containing compounds. However, because AMPA differs structurally from glyphosate, its surface coordination mode is expected to differ substantially from those proposed for glyphosate. Previous studies have demonstrated that the coordination configuration of glyphosate on mineral surfaces directly influences its degradation pathway and environmental persistence (Zhang et al., 2025), suggesting that elucidating the adsorption structure of AMPA is equally important.

Previous studies have suggested that AMPA adsorption on iron oxides is primarily controlled by coordination between the phosphonate group and surface Fe sites, whereas the amino group does not directly participate in surface complexation (Barja et al., 2005). Quantum chemical calculations have further shown that AMPA can adsorb onto graphene surfaces, and that transition-metal doping significantly enhances its adsorption affinity (Sacanamboy et al., 2024). Similar to glyphosate, AMPA adsorption also involves electrostatic interactions and hydrogen bonding with mineral surfaces (Wang et al., 2023). In addition, Ca^{2+} may promote adsorption through cation-bridging mechanisms during the adsorption of organophosphonate molecules. Nevertheless, the phosphonate group remains the dominant binding moiety, whereas the amino group plays little direct role in coordination with iron oxide surfaces (Zhang et al., 2025). Despite these advances, the molecular surface species, charge distribution, and corresponding surface complexation parameters for AMPA adsorption have not yet

been systematically established, and a unified surface complexation model is still lacking.

In natural environments, continuous degradation of organophosphonate compounds produces both AMPA and inorganic phosphate (PO_4^{3-}) (add references). Meanwhile, intensive agricultural fertilization and wastewater discharge introduce substantial amounts of phosphate into soils and aquatic systems. Consequently, competitive adsorption between AMPA and phosphate is expected to play a key role in determining the environmental mobility, retention, and bioavailability of AMPA. Because AMPA and phosphate possess similar phosphorus-containing coordination groups, it remains unclear whether they compete for identical surface sites and how differences in their molecular structures influence competitive adsorption behavior. The Charge Distribution Multi-Site Ion Complexation (CD-MUSIC) model integrates adsorption equilibria, surface complexation reactions, protonation states, and interfacial charge distribution into a unified theoretical framework (Hiemstra and Van Riemsdijk, 1996; Mendez and Hiemstra, 2019; Geysels et al., 2026), making it a powerful tool for predicting competitive adsorption processes between AMPA and phosphate and for elucidating their molecular adsorption mechanisms.

To our knowledge, no CD-MUSIC model has yet been developed for AMPA adsorption on ferrihydrite, and the molecular origin of competitive adsorption between AMPA and phosphate remains unresolved. In the present study, adsorption experiments, surface complexation modeling (SCM), and density functional theory (DFT) calculations were

combined to systematically investigate the molecular-scale adsorption mechanism of AMPA on ferrihydrite. Adsorption experiments were conducted over a wide range of pH values, surface loadings, and phosphate concentrations to elucidate the evolution of AMPA surface species under environmentally relevant conditions. The adsorption geometries and interfacial charge distributions optimized by DFT were employed to constrain the proposed surface complexes, while theoretical vibrational spectra were calculated to validate the adsorption configurations. Based on these results, a CD-MUSIC surface complexation model was established to quantitatively describe AMPA adsorption on ferrihydrite and to reveal the molecular mechanisms governing its retention at the mineral-water interface. The developed model provides a mechanistic framework for predicting the environmental fate, mobility, and bioavailability of AMPA in natural iron oxide systems.

2. Preparation and method

2.1 Synthesis of 6-lines ferrihydrite

6-line ferrihydrite was synthesized following the method described by Cornell and Schwertmann (2003). Briefly, 20 g of unhydrolyzed iron(III) nitrate nonahydrate ($Fe(NO_3)_3 \cdot 9H_2O$) was dissolved in 2.0 L of deionized water preheated to 75 °C under vigorous stirring. The solution was then transferred to an oven maintained at 75 °C and aged for 10-12 min. Subsequently, the solution was rapidly cooled in an ice-water bath. The resulting dark-red suspension was transferred into dialysis tubing (molecular weight cut-off: 3500 Da) and dialyzed against deionized water for 5-6 days until the electrical conductivity decreased to below 3.0 μS/cm. The purified suspension was

frozen and subsequently freeze-dried under vacuum (Labconco FreeZone, USA). The dried product was gently ground into a fine powder using an agate mortar and pestle and stored for subsequent adsorption experiments.

2.2 Adsorption of AMPA and Phosphate experiment

Stock solutions (54.5 mM) of phosphate and aminomethylphosphonic acid (AMPA) were prepared by dissolving sodium dihydrogen phosphate (NaH_2PO_4, Sinopharm Chemical Reagent Co., China) and aminomethylphosphonic acid (CH_6NO_3P, Alfa Aesar, USA), respectively, in deionized water. Appropriate volumes of the stock solutions were diluted to prepare individual phosphate solutions (1.07 and 0.54 mM), individual AMPA solutions (1.07, 0.86, 0.65, 0.54, 0.42, 0.31, 0.27, and 0.13 mM), as well as phosphate-AMPA mixed solutions at the desired concentrations. The pH of each solution was adjusted to the required range (3.5-10.5) using 0.1 M NaOH and HNO_3. Subsequently, 25 mL of each solution was transferred into a centrifuge tube, followed by the addition of 0.0600 g of ferrihydrite. The suspensions were shaken at 150 rpm for 24 h at 25 °C using an orbital shaker (Jinqi IS-RDS2C, China). After equilibration, the suspensions were centrifuged at 2.0×10^4 g for 10 min (Eppendorf 5810, Germany) and filtered through a 0.22 μm membrane filter. The filtrates were collected for the determination of total phosphorus and AMPA concentrations. Duplicate experiments were performed at the two extreme pH conditions (pH 3.5 and 10.5). The mean values and the corresponding upper and lower error limits were calculated to evaluate the possible variation in the experimental results.

2.3 Measure methodology of AMPA and Phosphate

AMPA concentrations in the supernatants were determined using a liquid chromatography-tandem mass spectrometry (LC-MS/MS) system consisting of a Shimadzu UHPLC coupled to a triple quadrupole mass spectrometer (QTRAP 6500+, Sciex). Chromatographic separation was achieved using an APP-HILIC column (5 μm, 2.1 × 100 mm, Waters), which is widely applied for the analysis of highly polar phosphonate compounds such as aminomethylphosphonic acid (AMPA) and glyphosate. The mobile phases consisted of ultrapure water (A) and acetonitrile (B), both containing 0.90 % formic acid. The gradient program started at 10 % A, increased linearly to 85 % A within 4 min, and was maintained for 11 min to ensure complete elution of AMPA. The flow rate was kept constant at 0.40 mL/min, and the column temperature was maintained at 35 °C. The injection volume was 10 μL. The mass spectrometer was operated in negative electrospray ionization (ESI-) mode. Typical source parameters included an ion spray voltage of -4.0 kV and a source temperature of 550 °C. Quantification was performed in multiple reaction monitoring (MRM) mode using optimized precursor/product ion transitions for AMPA. Calibration standards were prepared over the low micromolar concentration range, and samples were diluted appropriately to ensure that the measured concentrations fell within the linear calibration interval. Procedural blanks and calibration verification standards were analyzed periodically during the analytical sequence to confirm instrumental stability and analytical accuracy. The concentration of total phosphorus (P_{Total}) in the filtrate

was determined by inductively coupled plasma optical emission spectrometry (ICP-OES; iCAP 6500, Thermo Fisher Scientific, USA). The amount of phosphate adsorbed onto ferrihydrite ($PO_{4_{adsorbed}}$) was calculated according to the following equation:

$$PO_{4_{adsorbed}} = PO_{4_{initial}} - \ (P_{Total}\text{-}P_{AMPA})$$

In the above equation, $PO_{4_{initial}}$ denotes the initial phosphate concentration, P_{Total} is the total phosphorus concentration in the supernatant measured by ICP-OES, and $P_{AMPA}$is the AMPA concentration in the supernatant determined by LC-MS.

2.4 CD-MUSCI modeling

Based on the multisite ion complexation (MUSIC) model (Hiemstra, 1996), the crystal structure of ferrihydrite (Michel et al., 2010), and the corresponding surface structural models (Hiemstra et al., 2016; Mendez and Hiemstra, 2020), three types of reactive surface hydroxyl groups are present on the ferrihydrite surface, namely singly coordinated ($\equiv FeOH^{-0.5}$), doubly coordinated ($\equiv Fe_2OH^{0}$), and triply coordinated ($\equiv Fe_3OH^{-0.5}$) surface sites. In the present model, the surface site densities (N_s) of the singly and triply coordinated hydroxyl groups were assigned values of 3.6 and 2.7 sites/nm², respectively, corresponding to the 6-line ferrihydrite used in this study. Previous studies have reported different values for these site densities, including 3.0 and 2.8 sites/nm² (Hiemstra and Zhao, 2016), 5.8 and 1.4 sites/nm² (Mendez and Hiemstra, 2020), and 2.5 and 1.4 sites/nm² (Bram et al., 2026). In the present model,

only the singly coordinated surface hydroxyl groups were assumed to participate in ligand exchange reactions. The electrical double layer (EDL) was described using the extended Stern layer approach with a spherical double-layer geometry. The capacitances of the inner and outer Stern layers were fixed at 0.90 and 0.74 F/m² (C_1 and C_2, respectively), following the values commonly adopted for ferrihydrite. Previous X-ray absorption near-edge structure (XANES) spectroscopy studies, together with surface complexation modeling, have consistently demonstrated that glyphosate adsorbs onto ferrihydrite predominantly via inner-sphere complexation. Accordingly, both monodentate and bidentate surface complexes involving the phosphonate ($-PO_3$) and amino (-NH) functional groups were incorporated into the present model. The principal surface complexation reactions are given as follows:

$$\equiv FeOH^{-0.5} + AMPA^{3-}\ (aq) + H^{+}\ (aq) \rightleftharpoons \equiv FeOAMPA^{2-}\ (M) + H_2O\ (l) \quad (1)$$

$$\equiv FeOH^{-0.5} + AMPA^{3-}\ (aq) + 2H^{+}\ (aq) \rightleftharpoons \equiv FeOHAMPA^{2-}\ (MH) + H_2O\ (l) \quad (2)$$

$$\equiv FeOH + AMPA^{3-}\ (aq) + 3H^{+}\ (aq) \rightleftharpoons \equiv FeOH2AMPA^{0}\ (MH2) + H_2O\ (l) \quad (3)$$

$$2\equiv FeOH + AMPA^{3-}\ (aq) + 2H^{+}\ (aq) \rightleftharpoons \equiv (FeO)_2AMPA^{-}\ (B) + 2H_2O\ (l) \quad (4)$$

$$2\equiv FeOH + AMPA^{3-}\ (aq) + 3H^{+}\ (aq) \rightleftharpoons \equiv (FeO)_2HAMPA^{0}\ (BH) + 2H_2O\ (l) \quad (5)$$

In which, AMPA refers to the fully deprotonated species in aqueous solution. Although some studies distinguish the singly coordinated surface hydroxyl groups (≡FeOH) into a- and b-type sites, such subdivision has little influence on the numerical optimization of the surface complexation model. Therefore, no distinction between these two types of sites was made in the present study. Based on the surface complexation reactions (1)-(5), the adsorbed AMPA species on the ferrihydrite surface can be classified into mononuclear complexes (M), protonated mononuclear complexes (MH and MH_2), binuclear complexes (B), and protonated binuclear complexes (BH).

2.5 Quantum chemical optimization and charge distribution

The geometries of AMPA were optimized and analyzed using the Wavefunction module implemented in Spartan'04 (Devlin and Buch, 1997). The optimized molecular structures were subsequently interpreted according to the Brown bond valence concept (Brown and Altermatt, 1985). Geometry optimizations were performed using the LACVP+** (Los Alamos Core Valence Potentials) basis set available in Spartan. This basis set combines the 6-31+G** basis set with effective core potentials and was employed together with several density functional theory (DFT) functionals, including B3LYP, EDF2, ωB97X-D, and ωB97X-V, to optimize the molecular structures and evaluate the charge distribution.

Charge allocation for the ferrihydrite-AMPA surface complexes was established on the basis of the molecular binding geometry rather than applying a uniform charge

distribution. For the bidentate binuclear species (≡$(FeO)_2$AMPA and ≡$(FeO)_2$AMPAH), no residual charge was assigned to the outer Stern plane ($\Delta z_2 = 0$), indicating that the coordinated functional groups do not contribute additional electrostatic charge toward the solution. In contrast, the monodentate complex (≡FeOAMPAH) retains a negatively charged carboxylate moiety exposed to the aqueous phase; therefore, Δz_2 was fixed at -1. The optimized Δz_0 values were 0.55 ± 0.03, 0.74 ± 0.03, and 0.32 ± 0.02 for ≡$(FeO)_2$AMPA, ≡$(FeO)_2$AMPAH, and ≡FeOAMPAH, respectively. The remaining charge was subsequently assigned to the inner Stern plane by satisfying the overall charge balance of the adsorption reaction,

$$\Delta Z_1 = \Delta Z_{tot} - \Delta Z_0 - \Delta Z_2 \quad (6)$$

where Δz_{tot} represents the net charge introduced by the reacting AMPA species together with any associated protonation step. The calculated charge distribution coefficients are given in table 1.

Table 1. Calculated interfacial charge distribution coefficients (ΔZ_0 and ΔZ_1, v.u.) derived from MO/DFT-optimized geometries with dipole energy corrections using Eqs. (2) and (3) for a bidentate complex (B), a protonated bidentate complex (BH), and a protonated monodentate complex (MH_2).

Complex	B	BH	MH_2
n_0	0.46	0.69	0.28

Complex	B	BH	MH_2
n_1	-0.46	-0.69	-1.28
n_{H0}	0	0	0
n_{H1}	0	0	0
$\sum n_{ref}$	-1.0	-1.0	-0.50
Δz_0*	0.55	0.74	0.32
Δz_1*	-0.55	-0.74	-1.32

∗ includes dipoles correction using ϕ=0.17

The ionic charge distribution coefficients (n_0+n_{H0} and n_1+n_{H1}) was corrected for the electrostatic dipole effect. The correction results of the overall charge distribution coefficients (ΔZ_0 *and* ΔZ_1), which can be regarded as weighting factors in the multipole expansion of the interfacial electrostatic potential, were determined according to Hiemstra and van Riemsdijk (Hiemstra and van Riemsdijk, 2006) as:

$$\Delta Z_0 = n_0 + n_{H0} - \emptyset(n_0 + n_{H0} + \sum n_{ref} Z_{ref}) \quad (7)$$

And

$$\Delta Z_1 = n_1 + n_{H1} - \emptyset(n_0 + n_{H1} + \sum n_{ref} Z_{ref}) \quad (8)$$

In which n_0 and n_1 are the charge distributions to respectively the 0 and 1-plane of the ion species defined in the reaction equation, $\emptyset$ is the a proportionality constant

($\emptyset \sim 0.17$), n_{H0} and n_{H1} is the charge attributed to the 0- and 1-plane of any additional protons formulated in the reaction equation. Based on the optimized geometries and bond valence analysis, the dominant surface complexes were identified as binuclear (B), protonated binuclear (BH), and protonated mononuclear (MH_2) complexes. The final charge distribution values (ΔZ_0, ΔZ_1, and ΔZ_2) assigned to these surface complexes are summarized in Table 2.

Table 2 the surface species for Aminomethylphosphonic acid and phosphate with the charge distribution and the corresponding affinity constants (log K)

Species	≡FeOH	$\equiv Fe_3O$	ΔZ_0	ΔZ_1	ΔZ_2	logK†	Name
$\equiv(FeO)_2PO_2$	2	0	0.46	-1.46	0	29.77±0.02†	B
$\equiv FeOPO_2OH$	1	0	0.28	-1.28	0	27.65±0.01†	MH
$\equiv(FeO)_2AMPA$	2	0	0.55±0.03	-0.55±0.03	0	27.86±0.10	B
$\equiv(FeO)_2AMPAH$	2	0	0.74±0.03	-0.74±0.03	0	25.24±0.10	BH
≡FeOAMPAH	1	0	0.32±0.02	-1.32±0.02	-1.0	17.08±0.06	MH

† Stachowicz et al. (2008)

2.6 Charge distribution-Multi-Site Complexation (CD-MUSIC) modeling

The CD-MUSIC surface complexation model was implemented using the ECOSAT software package (Keizer and Van Riemsdijk, 1998), and the model parameters were optimized using FITEQL (Kinniburgh, 1993). Based on the established surface complexation framework and the optimized ferrihydrite surface parameters, the adsorption envelope data were fitted. The adsorption of AMPA was simulated using the

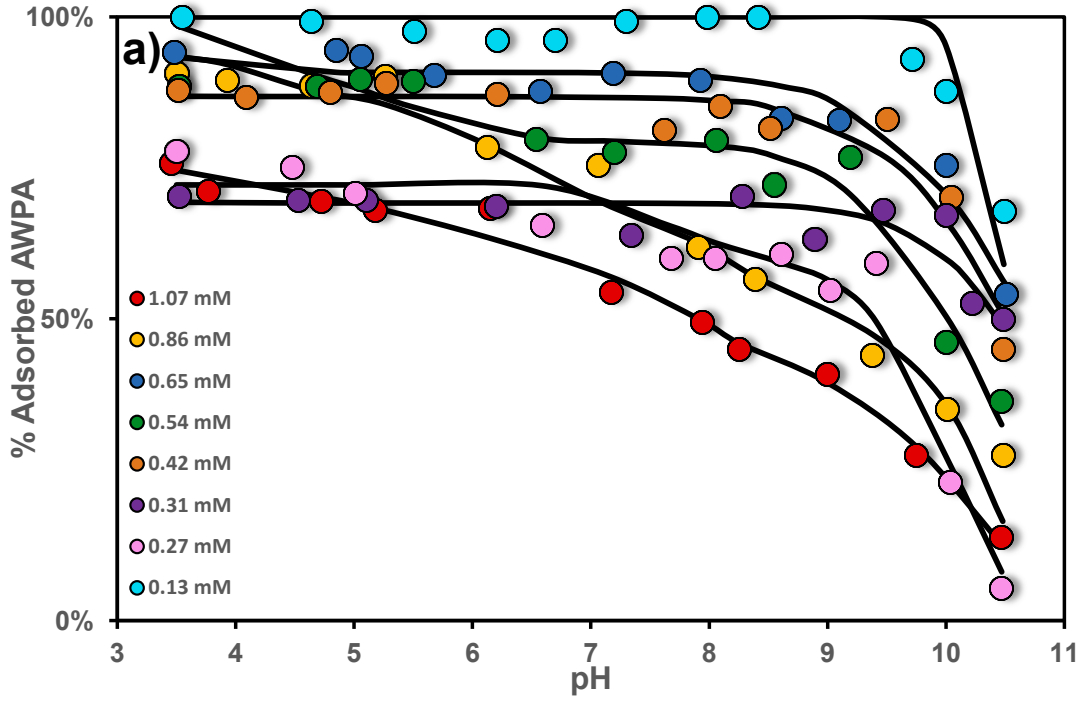
surface complexation reactions proposed in the present study, whereas phosphate adsorption was described using the bidentate surface complexes ≡$(FeO)_2PO_2$ and ≡$FeOPO_2OH$, as reported by Stachowicz et al. (2008). Adsorption was expressed as the percentage of solute adsorbed, and the experimental data were compared with the optimized model predictions.

3 Results and discussion

3.1 PMG adsorption to ferrihydrite

The adsorption envelopes of AMPA on 6-line ferrihydrite over the pH range of 3.5-10.5 at initial AMPA concentrations ranging from 0.13 to 1.07 mM was given in Fig.1a. The adsorption behavior was strongly affected by both solution pH and the initial AMPA concentration. Overall, adsorption was favored under acidic conditions and gradually decreased with increasing pH. However, the extent of this decrease depended strongly on the initial AMPA concentration. At acidic pH (3.5-5.5), ferrihydrite exhibited a high affinity for AMPA over the entire concentration range investigated. Adsorption exceeded approximately 85% for most systems with initial concentrations between 0.42 and 0.86 mM. At the lowest concentration (0.13 mM), AMPA was almost completely removed from solution, with adsorption remaining between 98 and 100% from pH 3.5 to 9.7. Even at pH 10.5, the adsorption percentage was still as high as 68%. The influence of pH became much more pronounced at higher initial concentrations. For an initial concentration of 1.07 mM, the adsorption percentage decreased continuously

from 76% at pH 3.5 to 54% at pH 7.2, followed by a further decrease to only 14% at pH 10.50. A similar trend was observed for the 0.86 mM system, where adsorption decreased from 91% to 27% over the investigated pH range. At intermediate concentrations (0.42-0.65 mM), the adsorption envelopes exhibited a different pattern. Adsorption remained relatively constant below approximately pH 8-9 and then decreased rapidly under alkaline conditions. For example, adsorption at 0.54 mM remained between 78 and 90% below pH 9.0 but decreased to 36% at pH 10.5. Likewise, adsorption at 0.42 mM remained close to 82-89% below pH 9.0 before declining to 45% at pH 10.5. Overall, the adsorption envelopes of AMPA on ferrihydirte shows that a strong pH dependency, quickly decreasing to at pH 9.0-9.5 (point of zero charge of 6-line ferrihydrite = 8.5). A similar pH-dependent adsorption behavior has previously been reported for ferrihydrite with phosphate alone (Hiemstra and Zhao, 2016) and glyphosate alone (Geysels et al., 2025; Geysels et al., 2026). In the present study, after normalizing the adsorption data by the initial AMPA concentration to construct the pH envelopes, a loading-dependent shift in the adsorption edge was observed. At low AMPA loadings (0.13 and 0.27 mM), adsorption decreased sharply at approximately pH 9.5. At intermediate loadings (0.42-0.65 mM), the sharp decrease occurred at around pH 9.0. In contrast, at high loadings (0.86 and 1.07 mM), no distinct adsorption edge was observed, and adsorption decreased gradually over the entire investigated pH range.



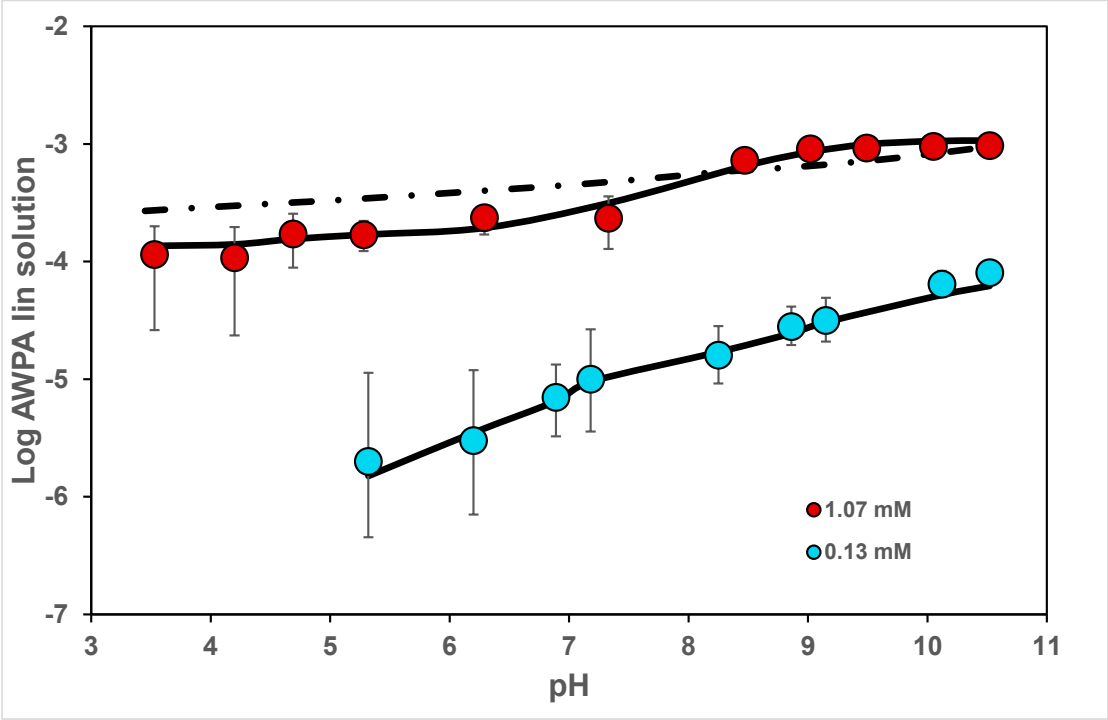


Fig. 1. Adsorption envelope of AMPA on 6-lines ferrihydrite as a function of pH. Panels (a) show the percentage adsorption and surface loading of AMPA, panel (b) presents the equilibrium AMPA concentration in solution for the two end-member adsorption system. Experiments were conducted using ferrihydrite suspensions with a background electrolyte of

0.010 M $NaNO_3$. Symbols represent the experimental measurements (average), and solid curves denote the predictions obtained from model. The dashed lines represent the model calculations for the systems without PO_4. Error bars represent the deviations of the maximum and minimum experimental values from the mean value.

The residual AMPA concentration in solution could also be successfully predicted using the CD-MUSIC model (Fig. 1b). Between the two extreme initial concentrations (1.07 mM and 0.13 mM), the residual AMPA concentration differed by as much as two orders of magnitude. In the presence of phosphate, the residual AMPA concentration increased (dashed lines in Fig. 1b), indicating competitive occupation of surface adsorption sites by phosphate. This competitive effect was more pronounced under acidic conditions.

3.2 Competitive adsorption of AMPA and PO_4^{3-}

3.2.1 1.07 mM phosphate

When 1.07 mM phosphate was present, the pH-dependent adsorption behavior of AMPA changed markedly (Fig. 2a). Compared with the phosphate-free system, phosphate reduced AMPA adsorption over the entire investigated pH range, although the extent of inhibition depended on both solution pH and the initial AMPA concentration. Under acidic conditions (pH < 6), the adsorption percentages remained close to 100% for all initial AMPA concentrations, indicating that the competitive effect of phosphate was negligible. In contrast, the inhibitory effect became pronounced under neutral to mildly alkaline conditions. For example, at an initial AMPA concentration of

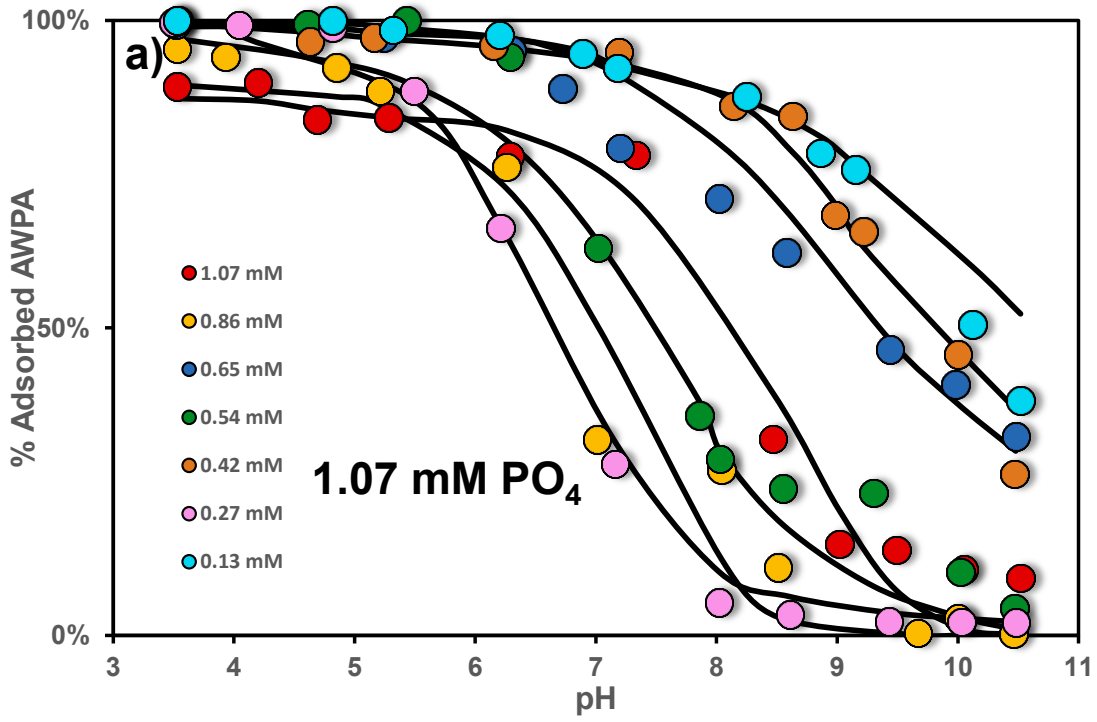
0.27 mM, the adsorption percentage decreased rapidly from approximately 66% at pH 6.2 to only 5% at pH 8.0, and AMPA adsorption was nearly eliminated at pH > 9. A similar trend was observed at higher AMPA concentrations, although the decrease was less pronounced, suggesting that phosphate primarily competes with AMPA for reactive surface sites on ferrihydrite.

The competitive effect of phosphate also depended on the initial AMPA concentration. At low AMPA loadings (0.13-0.27 mM), adsorption was almost completely suppressed under alkaline conditions, whereas a considerable fraction of AMPA remained adsorbed at higher loadings (0.65-1.07 mM). Compared with the phosphate-free system, the presence of phosphate shifted the entire adsorption envelope toward lower adsorption percentages, with the effect being particularly pronounced at low AMPA concentrations.

It is noteworthy that the adsorption envelopes did not change monotonically with increasing AMPA concentration. Instead, the highest adsorption percentages were observed at 0.13 and 0.42 mM AMPA, whereas the 1.07 mM system exhibited the lowest adsorption efficiency under acidic conditions, with adsorption remaining only about 84%. Nevertheless, increasing the AMPA concentration helped maintain relatively high adsorption efficiencies within the steeply declining region of the adsorption envelope (approximately pH 7.0-9.0). Comparison of the adsorption envelopes obtained in the presence and absence of phosphate further revealed that the addition of 1.07 mM phosphate substantially altered the adsorption behavior of AMPA. In particular, the adsorption envelope of 1.07 mM AMPA, which represented the lowest

adsorption boundary in the phosphate-free system, shifted toward the middle of the envelope bundle over the pH range of 6.0-9.0. Likewise, the adsorption envelope for 0.86 mM AMPA became much more similar to that of the 0.13 mM system. These observations suggest that phosphate not only competes directly with AMPA for adsorption sites but also modifies the surface charge characteristics of ferrihydrite, leading to a balance between competitive inhibition and electrostatic promotion.

The simulated phosphate adsorption envelopes are shown in Fig. 2b. Under different initial AMPA concentrations, the phosphate adsorption curves were confined within a relatively narrow band. The highest phosphate adsorption occurred under acidic conditions, ranging from 55% to 72%, whereas the lowest adsorption was observed under alkaline conditions, decreasing to 12-25%. Interestingly, the phosphate adsorption envelope at 0.42 mM AMPA was consistently located at the upper boundary of the adsorption band, which closely corresponded to the observation that the AMPA adsorption envelope at the same concentration approached the upper adsorption limit represented by the 0.13 mM system. This agreement further supports the hypothesis that the coupled effects of competitive adsorption and phosphate-induced surface electrostatic regulation jointly govern the adsorption behaviors of both phosphate and AMPA on ferrihydrite.



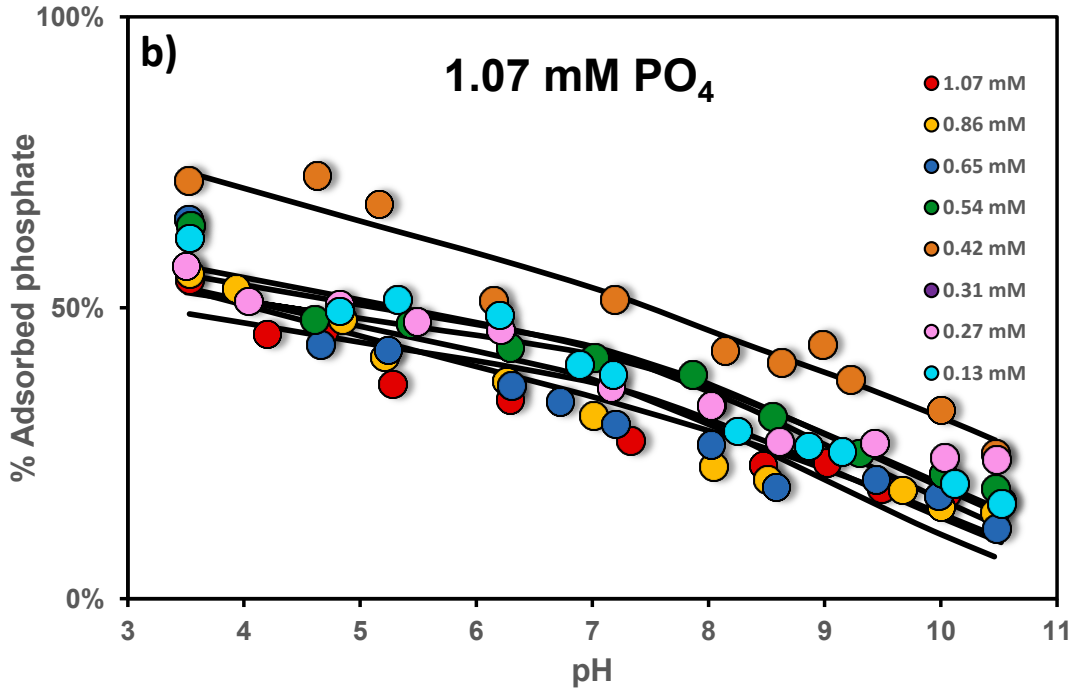


Fig. 2. Adsorption envelope of AMPA on 6-lines ferrihydrite as a function of pH. Panels (a) show the percentage adsorption and surface loading of AMPA with 1.07 mM phosphate concentration, panel (b) presents the percentage adsorption envelope of phosphate. Experiments were conducted using ferrihydrite suspensions with a background electrolyte of

0.010 M $NaNO_3$. Symbols represent the experimental measurements (average), and solid curves denote the predictions obtained from model, the dashed line represent the presence of phosphate.

Protonation induced by surface affinity interactions is considered to be one of the primary factors responsible for the pH changes observed before and after adsorption. In the single-AMPA adsorption system, the ΔpH curves exhibited two distinct regions (Fig.3). Under acidic to near-neutral conditions (pH < 8.0), AMPA adsorption mainly resulted in an increase in the solution pH, indicating the net consumption of protons (or equivalently, an increase in OH^- concentration). As the initial pH increased, the equilibrium pH gradually became lower than the corresponding initial pH, suggesting a transition from a predominantly deprotonation-dominated region to a protonation-dominated region (Fig.3). We appreciate that variations in solution pH alone cannot provide direct evidence for differences in the surface coordination configurations of the adsorbed species. Nevertheless, the ΔpH curves obtained at 0.42 and 0.13 mM AMPA were remarkably similar, which is consistent with the similarity observed in their adsorption envelopes. This agreement further indicates that the protonation and deprotonation behavior of reactive surface sites on ferrihydrite is closely associated with the amount of AMPA adsorbed.

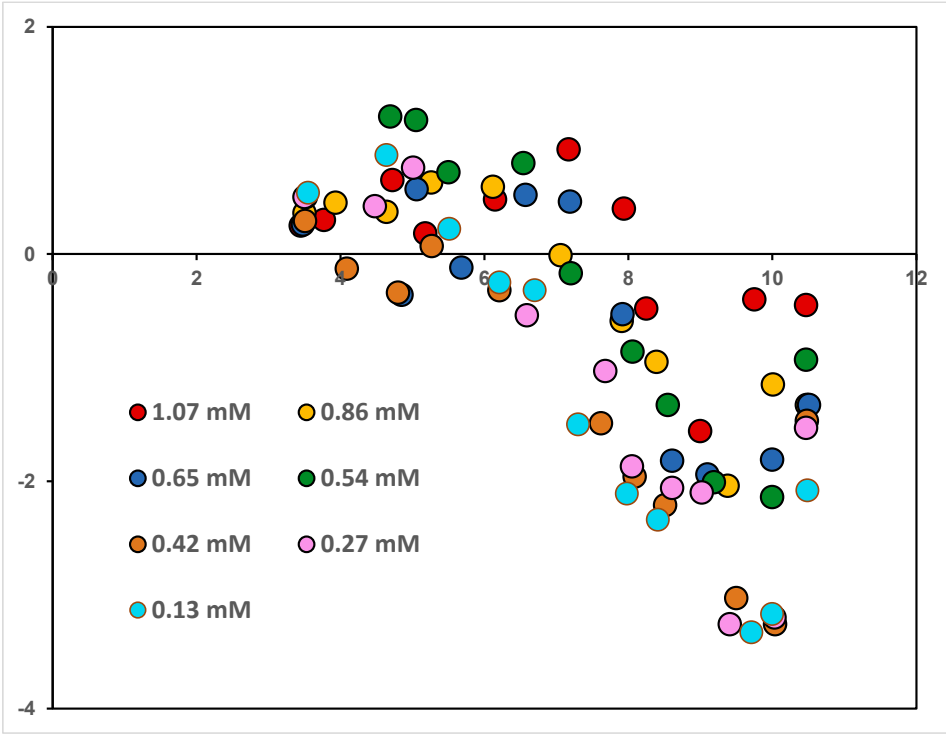


Fig. 3. Variation in pH (ΔpH) as a function of initial pH for the ferrihydrite-AMPA system before and after adsorption.

3.2.2 0.54 mM phosphate

Compared with the system containing 1.07 mM phosphate, the adsorption envelopes of AMPA obtained in the presence of 0.54 mM phosphate were considerably more similar to each other (Fig. 4a). For the low AMPA concentration range (0.13-0.42 mM), the adsorption percentage remained remarkably high, with a minimum value of approximately 95% over the entire pH range below 10. In contrast, the adsorption envelopes at higher AMPA concentrations exhibited a pronounced decline around the point of zero charge (PZC) of ferrihydrite. Unlike the system containing 1.07 mM phosphate, where the 0.27 mM AMPA adsorption envelope represented the lowest adsorption boundary, the 0.65 mM AMPA system exhibited the lowest adsorption

envelope in the presence of 0.54 mM phosphate. These results indicate that decreasing the concentration of the competing phosphate ions increases the lower boundary of the AMPA adsorption envelopes, thereby enabling a wider range of AMPA concentrations to maintain relatively high adsorption efficiencies.

The phosphate adsorption envelopes were also well reproduced by the surface complexation model (Fig. 4b). Under the lower phosphate loading (0.54 mM), the adsorption envelopes exhibited a more monotonic dependence on the initial AMPA concentration. Specifically, the adsorption percentage of phosphate increased progressively as the initial AMPA concentration decreased. For example, the maximum phosphate adsorption was approximately 67% at an initial AMPA concentration of 1.07 mM, whereas phosphate adsorption approached nearly complete removal at 0.13 mM AMPA. Interestingly, however, the 0.86 mM AMPA system exhibited the lowest phosphate adsorption percentage among all investigated systems. This behavior suggests that, in addition to electrostatic inhibition, electrostatic regulation of the ferrihydrite surface may also influence the competitive adsorption process. A similar phenomenon can also be observed in the adsorption envelopes obtained at the higher phosphate concentration (1.07 mM, Fig. 2b), where the phosphate adsorption curves corresponding to 1.07 and 0.86 mM AMPA were both located near the lower boundary.

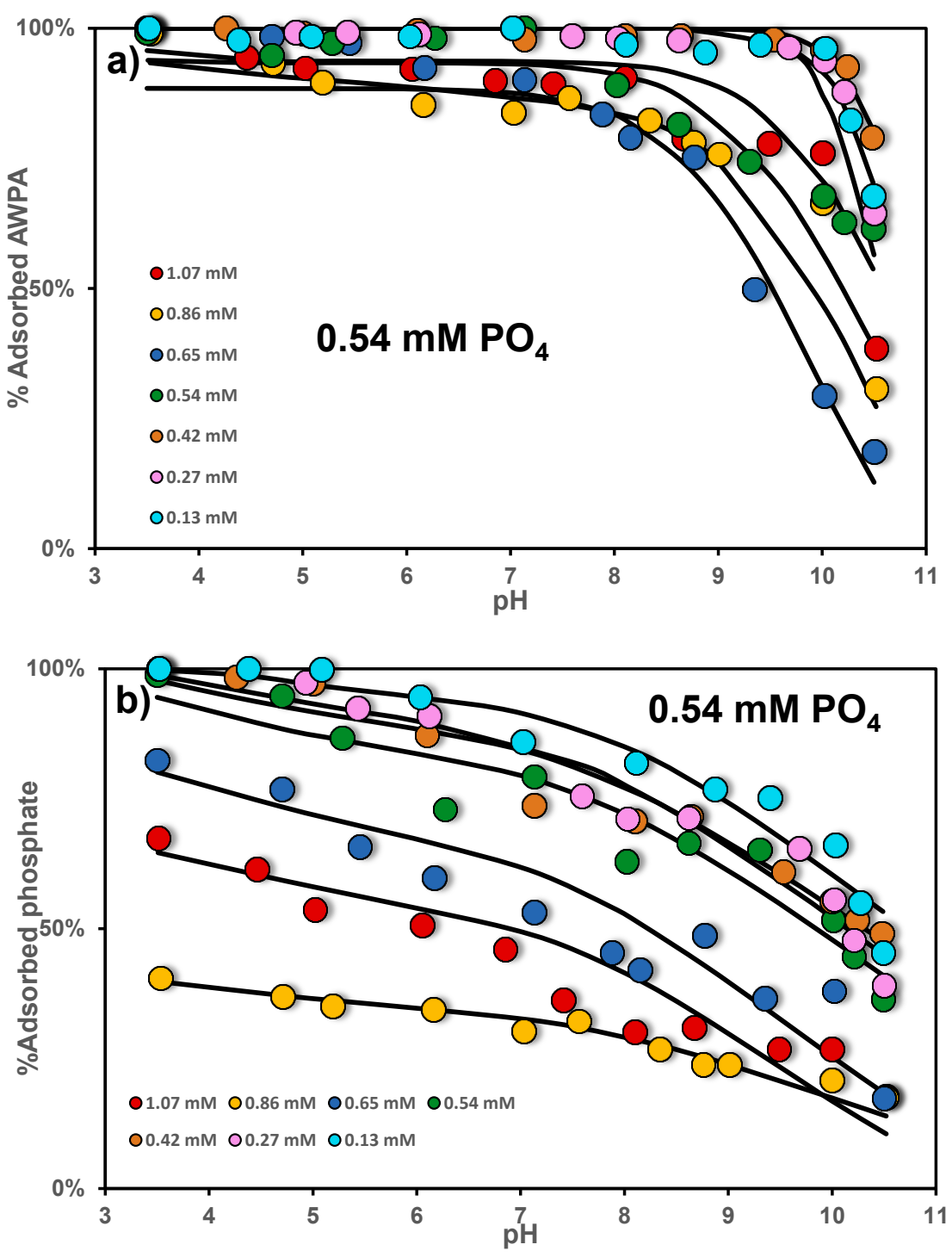


Fig. 4. Adsorption envelope of AMPA on 6-lines ferrihydrite as a function of pH. Panels (a) show the percentage adsorption and surface loading of AMPA with 0.54 mM phosphate concentration, panel (b) presents the percentage adsorption envelope of phosphate. Experiments were conducted using ferrihydrite suspensions with a background electrolyte of

0.010 M $NaNO_3$.

3.3 affinity comparison of AMPA and PO_4^{3-} on ferrihydrite

For two-ion competitive systems, the CD model is able to achieve good predictive performance. Although phosphate exhibits slightly higher intrinsic affinity constants (log K = 27.7-29.8) than the dominant bidentate AMPA complex (log K = 27.9), phosphate introduces substantially more negative charge into the first Stern plane (Δz_1 = -1.28 to -1.46), whereas the dominant AMPA bidentate complexes exhibit much smaller first-plane charge contributions (Δz_1 = -0.55 to -0.74). Consequently, phosphate adsorption induces a much stronger increase in the electrostatic penalty associated with the ψ_1 potential, progressively suppressing subsequent phosphate adsorption. In contrast, the dominant AMPA complexes perturb the Stern-layer potential to a much lesser extent, allowing AMPA to maintain a relatively higher adsorption level despite direct competition for surface sites. This interpretation is consistent with the experimentally observed AMPA/PO_4 adsorption ratio, which increased from approximately 1.0 at pH 3.5 to 1.7 at pH 10.5. These results suggest that competitive adsorption is governed not only by intrinsic affinity and site competition but also by the different charge distributions of the surface complexes and their feedback on the Stern-layer electrostatic potential. Macroscopically, AMPA exhibited stronger adsorption behavior toward ferrihydrite than phosphate.

4 Conclusions

In this study, the adsorption of aminomethylphosphonic acid (AMPA) and phosphate on ferrihydrite was investigated. The MUSIC model was applied to establish the primary charging behavior of the surface complexes, which was subsequently used to predict competitive adsorption in complex systems. The main conclusions are summarized as follows:

AMPA adsorbs onto the ferrihydrite surface mainly as three surface complexes: a bidentate complex (B), a protonated bidentate complex (BH), and a protonated monodentate complex (MH), with corresponding intrinsic equilibrium constants (log K) of 27.9 ± 0.10, 25.3 ± 0.10, and 17.1 ± 0.06, respectively. The CD values of the AMPA and phosphate surface complexes were independently derived from MO/DFT-optimized geometries of the hydrated complexes. The resulting model successfully reproduced the competitive adsorption experiments through iterative fitting of the ferrihydrite adsorption envelope data.

The presence of phosphate significantly altered the adsorption edge of AMPA. Owing to the pH-dependent adsorption behavior of ferrihydrite, the residual AMPA concentrations at the two extreme initial AMPA concentrations (0.13 and 1.07 mM) differed by as much as two orders of magnitude. Compared with phosphate, AMPA exhibited a stronger affinity for the ferrihydrite surface. At identical initial concentrations, the maximum amount of adsorbed AMPA was 1.7z times that of phosphate. The adsorption behavior of AMPA and phosphate was governed by the

combined effects of competitive inhibition and electrostatic promotion at the mineral surface, rather than being determined solely by pH or the initial solute concentration.

Acknowledgements

We gratefully acknowledge Bram Geysels of Wageningen University for valuable help on CD-MUSIC model.

Funding

This work was supported by the Sichuan Province Science and Technology Support Program (2024ZYD0042).

Authors' Contributions

Jing LIU: Writing – original draft, review & editing, Data curation, Visualization, Validation, Methodology, Investigation, Funding acquisition, Conceptualization.

Shu Chen: Writing – review & editing, Visualization, Funding acquisition, Project administration, Resource.

Ethical Approval

This is not applicable.

Consent to Participate

This is not applicable.

Consent to Publish

This is not applicable.

Competing Interests

The authors declare that they have no competing interests.

Data Availability Statement

The data supporting the findings of this study are available from the corresponding author upon reasonable request.

References

Barja, B.C., dos Santos Afonso, M., 2005. Aminomethylphosphonic acid and glyphosate adsorption onto goethite: A comparative study. Environ. Sci. Technol. 39 (2), 585–592. https://doi.org/10.1021/es035055q

Barrett, K.A., McBride, M.B., 2005. Oxidative degradation of glyphosate and aminomethylphosphonate by manganese oxide. Environ. Sci. Technol. 39 (23), 9223–9228. https://doi.org/10.1021/es051342d

Cicilinski, A.D., Peralta-Zamora, P., 2025. Glyphosate and AMPA sorption onto synthetic iron (oxyhydr)oxides: A comparative study. J. Mol. Liq. 426, 127303. https://doi.org/10.1016/j.molliq.2025.127303

Daniel Villalobos-Lara, A., Rivera-Iturbe, F.F., Gamiño-Arroyo, Z., et al., 2026. Experimental and CFD simulation of glyphosate dephosphorylation by active chlorine electrosynthesis in a flow reactor. J. Appl. Electrochem. 56 (8), 145. https://doi.org/10.1007/s10800-026-02528-w

Geysels, B., Hiemstra, T., Groenenberg, J.E., Comans, R.N.J., 2025. Glyphosate binding and speciation at the water-goethite interface: A surface complexation model consistent with IR spectroscopy and MO/DFT. Water Res. 273, 123031. https://doi.org/10.1016/j.watres.2024.123031

Geysels, B., Hiemstra, T., Vermeer, A.W.P., Groenenberg, J.E., 2026. A mechanistic surface complexation model for glyphosate adsorption to ferrihydrite in competition with phosphate. Water Res. 288, 124634. https://doi.org/10.1016/j.watres.2025.124634

Grandcoin, A., Piel, S., Baurès, E., 2017. Aminomethylphosphonic acid (AMPA) in natural waters: Its sources, behavior and environmental fate. Water Res. 117, 187–197. https://doi.org/10.1016/j.watres.2017.03.055

Hiemstra, T., Van Riemsdijk, W.H., 1996. A surface structural approach to ion adsorption: The charge distribution (CD) model. J. Colloid Interface Sci. 179 (2), 488–508.

Lescano, M.R., Pizzuti, L., Castillo, M.P., Zalazar, C.S., 2018. Glyphosate and aminomethylphosphonic acid degradation in biomixtures based on alfalfa straw, wheat stubble and river waste. J. Environ. Manage. 228, 451–457. https://doi.org/10.1016/j.jenvman.2018.09.009

Li, H., Joshi, S.R., Jaisi, D.P., 2016. Degradation and isotope source tracking of glyphosate and aminomethylphosphonic acid. J. Agric. Food Chem. 64 (3), 529–538. https://doi.org/10.1021/acs.jafc.5b04838

Mendez, J.C., Hiemstra, T., 2019. Carbonate adsorption to ferrihydrite: Competitive interaction with phosphate for use in soil system. ACS Earth Space Chem. 3 (1), 129–141. https://doi.org/10.1021/acsearthspacechem.8b00160

Pereira, R.C., Anizelli, P.R., Di Mauro, E., et al., 2019. The effect of pH and ionic strength on the adsorption of glyphosate onto ferrihydrite. Geochem. Trans. 20 (1), 3. https://doi.org/10.1186/s12932-019-0063-1

RAMPAzzo, N., RAMPAzzo Todorovic, G., Mentler, A., Blum, W.E.H., 2013. Adsorption of glyphosate and aminomethylphosphonic acid in soils. Int. Agrophys. 27, 203–209. https://doi.org/10.2478/v10247-012-0086-7

Ruffolo, F., Dinhof, T., Murray, L., Zangelmi, E., Chin, J.P., Pallitsch, K., Peracchi, A., 2023. The microbial degradation of natural and anthropogenic phosphonates. Molecules 28 (19), 6863. https://doi.org/10.3390/molecules28196863

Sacanamboy, D.S., Quispe-Corimayhua, L., Tilvez, E.A., Yáñez, O., 2024. Adsorption of aminomethylphosphonic acid on pristine graphene and graphene doped with transition metals: A theoretical study. Chem. Phys. Lett. 850, 141481. https://doi.org/10.1016/j.cplett.2024.141481

Singh, B.K., Walker, A., 2006. Microbial degradation of organophosphorus compounds. FEMS Microbiol. Rev. 30 (3), 428–471. https://doi.org/10.1111/j.1574-6976.2006.00018.x

Stachowicz, M., Hiemstra, T., van Riemsdijk, W.H., 2008. Multi-competitive

interaction of As(III) and As(V) oxyanions with Ca^{2+}, Mg^{2+}, PO_4^{3-} and CO_3^{2-} ions on goethite. J. Colloid Interface Sci. 320 (2), 400–414. https://doi.org/10.1016/j.jcis.2008.01.007

Sun, M., Li, H., Jaisi, D.P., 2019. Degradation of glyphosate and bioavailability of phosphorus derived from glyphosate in a soil-water system. Water Res. 163, 114840. https://doi.org/10.1016/j.watres.2019.07.007

Trinh, P.B., Liu, S., Himma, N.F., Fiser, B., Schäfer, A.I., 2026. Continuous-flow photocatalytic degradation of glyphosate and aminomethylphosphonic acid under simulated sunlight with TiO2-coated poly(vinylidene fluoride) membrane. Adv. Funct. Mater. 36 (21), e11431. https://doi.org/10.1002/adfm.202511431

Wang, M., Rivenbark, K.J., Phillips, T.D., 2023. Adsorption and detoxification of glyphosate and aminomethylphosphonic acid by montmorillonite clays. Environ. Sci. Pollut. Res. 30 (5), 11417–11430. https://doi.org/10.1007/s11356-022-22927-8

Zhang, M., Zhao, W., Li, X., Ma, H., Feng, X., Tan, W., Wang, X., 2026. Synergistic adsorption of glyphosate and calcium on ferrihydrite: Molecular insights into herbicide fate in soils. Soil Environ. Health 4, 100218. https://doi.org/10.1016/j.seh.2026.100218

Zhang, N., Sun, H., Zhan, G., Zu, J., Zhang, L., 2025. Green glyphosate treatment with ferrihydrite and CaO2 via forming surface ternary complex. Environ. Sci. Technol. 59, 2791–2801. https://doi.org/10.1021/acsesst.4c10882